PIER C

(Received 3 July 2024, Accepted 6 August 2024, Scheduled 21 August 2024)

A Planar Sharp-Attenuation Ultra-Wideband Bandstop Filter with a Three Section Coupled-Line Stub

Mengxin He[1,2], Xiaoying Zuo[1,2,*], Hang Mei[1,2], and Yajian Li[1,2]

[1] *Beijing Key Laboratory for Sensor, Beijing Information Science & Technology University, Beijing 100192, China*
[2] *School of Applied Science, Beijing Information Science & Technology University, Beijing 100192, China*

ABSTRACT: A novel design of a sharp-attenuation ultra-wideband bandstop filter (BSF) is presented in this paper, which is composed of two transmission lines (TLs) and four pairs of coupled-lines. The five transmission zeros in the stopband can improve the bandwidth and roll-off factor of the filter. To verify the design, the filter is manufactured on printed circuit board (PCB), and its performance is measured. The 10-dB stopband insertion loss bandwidth of the filter is 0.45–3.76 GHz (relative bandwidth 157%), with good frequency selectivity. The 20-dB attenuation rate on the lower side of the stopband is about 154.5 dB/GHz.

1. INTRODUCTION

The ubiquitous abundance of wireless communication leads to a concern about the electromagnetic interference. How to avoid electromagnetic interference is a hot issue. Ultra-wideband (UWB) band-stop filters equipped with high performance could efficiently avoid electromagnetic interference. Many novel studies on wide/ultra-band band-stop filters have been reported. Structural innovations attain wide/ultra-band band-stop filters [1–4], such as coupled-line with a single-ended ground [1], circularly etched stub [2], symmetrical three-layer ring structure [3], and double split ring resonator [4]. In [5], open-circuited stubs are implemented to design a UWB filter, and the selectivity is optimized by adjusting the stub size, for example half-wavelength or quarter-wavelength. A new type of resonator feeding with four directors distributed line is studied, and a compact UWB band-stop filter is achieved. TZs are created by folding open stubs [6]. Meanwhile, stepped-impedance open stubs enhance the rejection depth as referred from [7]. Dual/multi-band band-stop filters usually suppress unwanted double/multi (side) band signals such as in amplifiers and mixers systems [8–10]. In [10], a stub-enclosed stepped-impedance resonator is embedded to form a compacted dual-wideband band-stop filter. A T-shaped defected microstrip structure (DMS) [11] and annular shaped stubs [12] are embedded in multi-band band-stop filters. The technology of passive circuits implementing UWB filters as introduced above has been frequently reported. However, active circuits can also realize UWB band-stop filters [13], and variable capacitive diode is often used to tune the stopband bandwidth. In [14], a single layer ultra-wideband frequency selective surface with square (UWB FSS) loop and cross dipole structure is proposed for shielding application. This FSS covers 4.85 GHz to 17.2 GHz at 10 dB insertion loss.

In this work, a sharp-attenuation ultra-wideband band-stop filter is proposed, which consists of two transmission lines and four pairs of coupled-lines. The transmission zero in the stopband makes its performance better. Compared to the relevant proposed structure, this filter has a wider stopband and steeper 20-dB attention rate (AR). After measurement, the relative 10-dB bandwidth of the filter is 157%, and a very steep AR of 154.5 dB/GHz is achieved.

2. CIRCUIT CONFIGURATION AND DESIGN THEORETICAL ANALYSIS

2.1. Design Analysis

The schematic of the wideband BSF is shown in Fig. 1(a). The left part of BSF consists of two TLs and a pair of coupled-lines. Three pairs of coupled-lines are connected in series to form the right part. For analysis, the characteristic impedances of odd- and even-mode of the coupled-lines are assumed as Z_{ei}

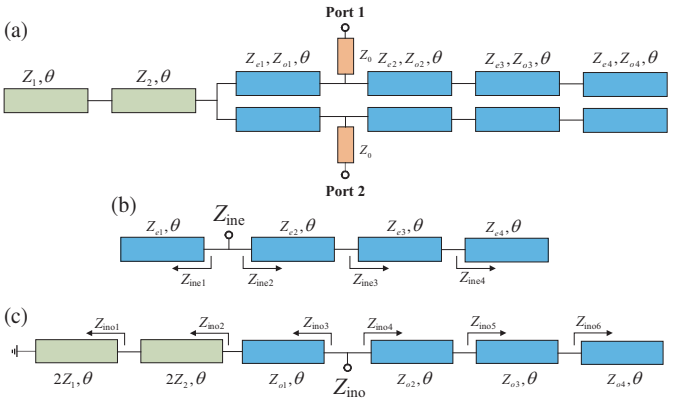

FIGURE 1. The (a) schematic of the proposed wideband BPF, (b) even-mode and (c) odd-mode equivalent circuit.

* Corresponding author: Xiaoying Zuo (zuoxiaoying03@163.com).

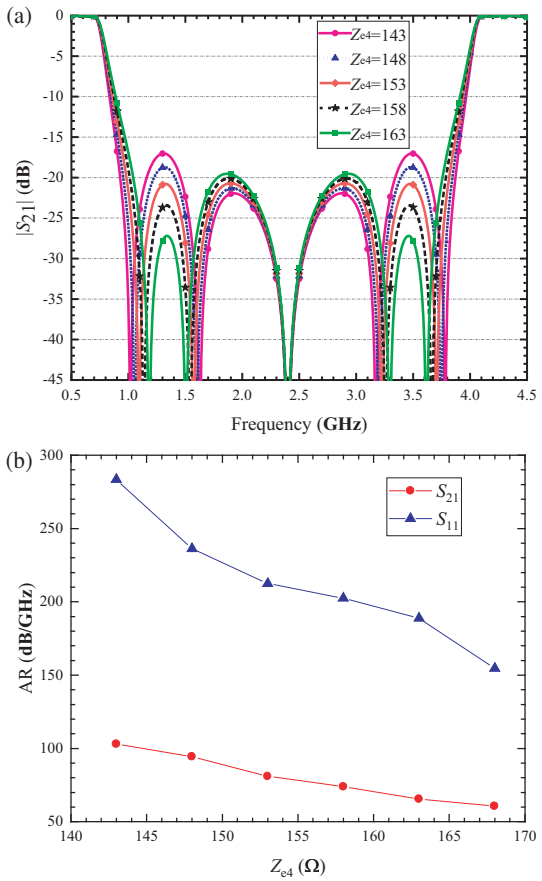

FIGURE 2. The (a) S_{21} simulation curves under different Z_{e4}, (b) relationship between AR and Z_{e4}.

and Z_{oi} $(i = 1, 2, 3, 4)$, respectively, while the characteristic impedances of the transmission lines are Z_1 and Z_2. Their electric lengths are all defined as θ.

Even- and odd-mode analysis is used for the schematic since the structure is symmetric. The even-mode and odd-mode equivalent circuit of band-stop filter is shown in Fig. 1(b) and Fig. 1(c). Z_{ino} and Z_{ine} respectively represent the input impedance under parity excitation.

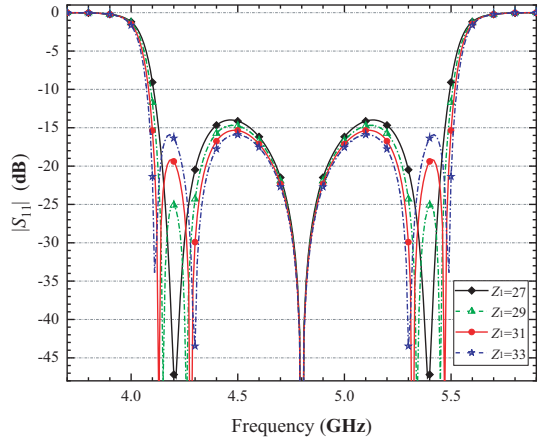

FIGURE 3. TPs positions in upper pass band versus Z_1.

According to [15], Z_{ine1}, Z_{ine2}, Z_{ine3} and Z_{ine4} are

$$\begin{cases} Z_{ine1} = -jZ_{e1}\cot\theta \\ Z_{ine2} = j\frac{\left(Z_{e2}^2Z_{e3}+Z_{e2}^2Z_{e4}+Z_{e2}Z_{e3}^2\right)\tan^2\theta - Z_{e2}Z_{e3}Z_{e4}}{-Z_{e3}^2\tan^3\theta+(Z_{e2}Z_{e3}+Z_{e2}Z_{e4}+Z_{e3}Z_{e4})\tan\theta} \\ Z_{ine3} = j\frac{Z_{e3}^2\tan^2\theta - Z_{e3}Z_{e4}}{(Z_{e3}+Z_{e4})\tan\theta} \\ Z_{ine4} = -jZ_{e4}\cot\theta \end{cases} \tag{1}$$

Similarly, Z_{inoi} $(i = 1, 2, 3, 4, 5)$ are calculated as

$$\begin{cases} Z_{ino1} = 2jZ_1\tan\theta \\ Z_{ino2} = 2jZ_2\frac{(Z_1+Z_2)\tan\theta}{-Z_1\tan^2\theta+Z_2} \\ Z_{ino3} = jZ_{o1}\frac{Z_1Z_{o1}\tan^3\theta - Z_2(2Z_1+2Z_2+Z_{o1})\tan\theta}{\left(Z_1Z_{o1}+2Z_2^2+2Z_1Z_2\right)\tan^2\theta - Z_2Z_{o1}} \\ Z_{ino4} = jZ_{o2}\frac{\left(Z_{o2}Z_{o3}+Z_{o2}Z_{o4}+Z_{o3}^2\right)\tan^2\theta - Z_{o3}Z_{o4}}{-Z_{o3}^2\tan^3\theta+(Z_{o2}Z_{o3}+Z_{o2}Z_{o4}+Z_{o3}Z_{o4})\tan\theta} \\ Z_{ino5} = j\frac{Z_{o3}^2\tan^2\theta - Z_{o3}Z_{o4}}{(Z_{o3}+Z_{o4})\tan\theta} \\ Z_{ino6} = -jZ_{o4}\cot\theta \end{cases} \tag{2}$$

Z_{ine} and Z_{ino} are

$$Z_{ine} = \frac{Z_{ine1}Z_{ine2}}{Z_{ine1}+Z_{ine2}} \tag{3a}$$

$$Z_{ino} = \frac{Z_{ino3}Z_{ino4}}{Z_{ino3}+Z_{ino4}} \tag{3b}$$

The S-parameters are as follows:

$$S_{11} = \frac{Z_0^2 - Z_{ine}Z_{ino}}{(Z_{ino}+Z_0)(Z_{ine}+Z_0)} \tag{4a}$$

$$S_{21} = \frac{Z_0(Z_{ine}-Z_{ino})}{(Z_{ino}+Z_0)(Z_{ine}+Z_0)} \tag{4b}$$

To obtain the stopband, setting $S_{21} = 0$. Taking the derivation of (4), gives the following equation of $\tan^2\theta$.

$$A_4\left(\tan^2\theta\right)^4 + A_3\left(\tan^2\theta\right)^3 + A_2\left(\tan^2\theta\right)^2 + A_1\tan^2\theta + A_0 = 0 \tag{5}$$

Through Equation (5), the TZs positions in the stopband and bandwidth can be derived.

2.2. Parameter Analysis and Optimization

According to [9], 20-dB attenuation rate is defined as

$$AR = \frac{20\,\text{dB} - 3\,\text{dB}}{|f_{20\,\text{dB}} - f_{3\,\text{dB}}|} \tag{6}$$

By adjusting the parameters in the original design, the performance of the filter can be optimized. As shown in Fig. 2(a), the bandwidth and AR of the filter vary with the value of Z_{e4}. When Z_{e4} decreases from 163 to 143, the width of stopband becomes wider, but the stopband rejection becomes worse. The AR under each Z_{e4} is calculated separately, as shown in

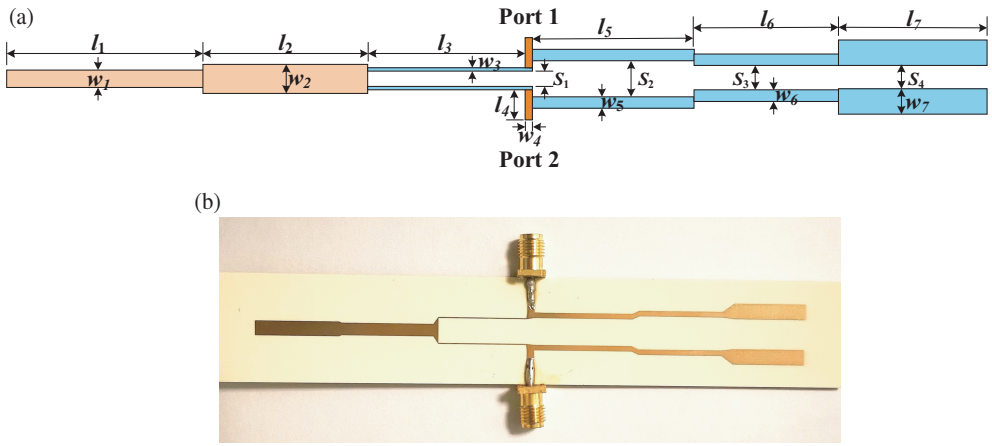

FIGURE 4. The (a) layout with physical dimensions and (b) the photograph of the sharp-attenuation ultra-wideband bandstop filter.

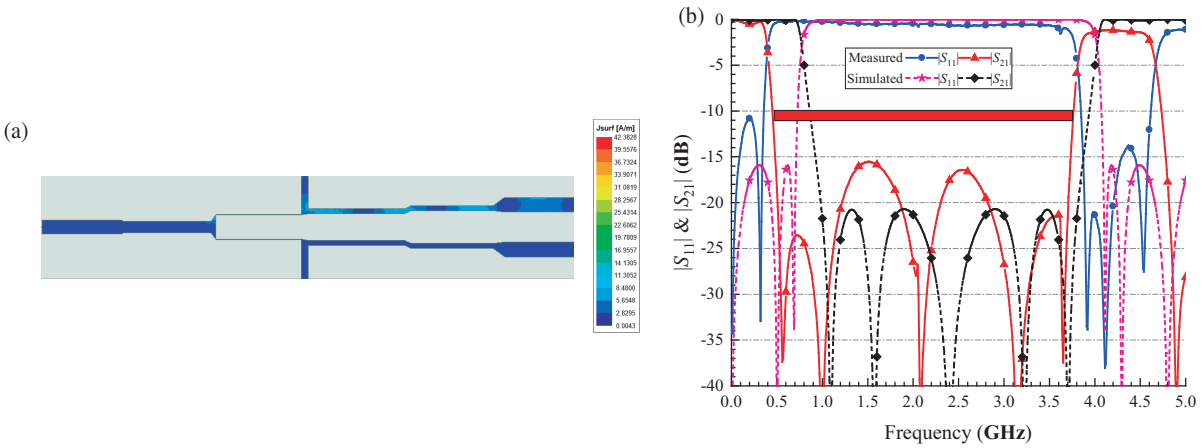

FIGURE 5. The (a) current distribution across the design and (b) the simulated and measured scattering parameters.

Fig. 2(b). Smaller values of Z_{e4} offer better frequency selectivity and sharper stopband attenuation.

After discussing the roll-off factor, transmission poles (TPs) can be obtained by setting $S_{11} = 0$. For BSFs, out-of-band TPs are very important. The passband transmission of the filter preforms better with more out-of-band TPs. In the process of simulation, it is found that the transmission poles are mainly controlled by two short transmission lines. Fig. 3 shows that when Z_1 increases from 27 to 33, the number of transmission poles in the upper passband increases from 3 to 5, and the input reflection coefficient decreases. Properly increasing the value of Z_1 can enhance the performance stability of the filter.

The final parameters are as follows: $Z_1 = 33\,\Omega$, $Z_2 = 26\,\Omega$, $Z_{e3} = 100\,\Omega$, $Z_{e1} = 155\,\Omega$, $Z_{o1} = 118\,\Omega$, $Z_{e2} = 62\,\Omega$, $Z_{o2} = 45\,\Omega$, $Z_{e3} = 148\,\Omega$, $Z_{o3} = 98\,\Omega$, $Z_{e4} = 153\,\Omega$, $Z_{o4} = 92\,\Omega$, $\theta = 90°$.

3. FULL-WAVE SIMULATION AND EXPERIMENTAL MEASUREMENT

According to the analysis and calculation in Section 2, the layout of the wideband BSF is designed, as shown in Fig. 4(a).

TABLE 1. Physical size of the proposed BSF (unit: mm).

l_1	w_1	l_2	w_2	l_3	w_3	s_1	l_4
19	3.3	20.5	2.8	20	0.2	5.7	22.5
w_4	s_2	l_5	w_5	s_3	l_6	w_6	s_4
1.2	6.2	19.2	1.2	7.7	16.4	7	3.5

The final physical size of each line is given in Table 1. The proposed circuit structure is designed and fabricated on a Rogers RO4350B substrate with dielectric constant ($\varepsilon_r = 3.66$), loss tangent ($\tan\theta = 0.0037$), substrate height ($h = 0.762\,\text{mm}$), and the copper material thickness is 0.035 mm. A photo of the fabricated bandstop filter is shown in Fig. 4(b). The S-parameters are measured by using a vector network analyzer.

Figure 5(a) shows the current distribution across the design. In Fig. 5(b), the proposed BSF's simulated and measured results achieve well. The measured stopband 10-dB insertion loss bandwidth is 157% (0.45 GHz–3.76 GHz), and the center frequency is 2.105 GHz. The required five transmission zeros are 0.56, 1.0, 2.08, 3.15, 3.65 GHz. According to formula (6), the 20-dB attenuation rate of the BSF can be ob-

tained. The ARs on the lower and upper sides of the stopband are about 154.5 dB/GHz and 130.8 dB/GHz. The simulated results agree well with the measured ones. The core circuit size is $1.49\lambda_g \times 0.29\lambda_g$ (125.25 mm × 24.6 mm) (λ_g: the guided wavelength at the center frequency).

Finally, Table 2 shows the performance comparison with other wideband band-stop filters reported in the prior studies. Compared with other literatures, the proposed filter has larger relative bandwidth and sharper stopband attenuation.

TABLE 2. Performance comparison with previous works.

Ref.	TZs	f_0 (GHz)	FBW (%)	Upper AR (dB/GHz)	Size ($\lambda_g \times \lambda_g$)
[1]	5	1.96	68.4	-	0.23×0.31
[2]	3	6.57	~ 90.4	47.2	0.219×0.410
[3]	5	1.5	122.5	230.8	0.062
[7]	5	2.0	88.5	106.3	0.31
This work	5	2.1	157	130.8	0.432

TZs: transmission zeros, f_0: center frequency, FBW: fractional bandwidth, AR: attenuation rate.

4. CONCLUSION

A new wideband band-stop filter circuit structure is proposed. The filter is composed of two transmission lines and four pairs of coupled-lines, which can generate five transmission zeros in the stopband. The TZs have a significant impact on the performance of the filter. The filters have achieved many remarkable advantages including ultra-bandwidth and sharp-attenuation with good frequency selectivity. The design of circuit structure is analyzed and fabricated on PCB. The full wave test results validate the correctness of the design method. These filters can be used in wireless communication systems.

ACKNOWLEDGEMENT

This work was supported by the National Natural Science Foundation of China (62201065).

APPENDIX A.

A_0, A_1, A_2, A_3, A_4 in formula (5) are as follows:

$$A_0 = Z_2 Z_{e1} Z_{e2} Z_{e3} Z_{e4} Z_{o1} Z_{o2} Z_{o3} Z_{o4} \tag{A1}$$

$$\begin{aligned} A_1 = & -Z_{o1} Z_{o2} Z_2 Z_{o3} Z_{o4} \left(2Z_1 + 2Z_2 + Z_{o1}\right) \\ & \left(Z_{e2} Z_{e3} Z_{e4} + Z_{e1} \left(Z_{e2} Z_{e3} + Z_{e2} Z_{e4} + Z_{e3} Z_{e4}\right)\right) \\ & -Z_{e1} Z_{e2} Z_{e3} Z_{e4} \\ & \left(\begin{array}{l} Z_{o1} Z_2 \left(2Z_1 + 2Z_2 + Z_{o1}\right) \\ \left(Z_{o2} Z_{o3} + Z_{o2} Z_{o4} + Z_{o3} Z_{o4}\right) \\ +Z_{o2} \left(Z_2 Z_{o1} \left(Z_{o2} Z_{o3} + Z_{o2} Z_{o4} + Z_{o3}^2\right)\right. \\ \left. +Z_{o3} Z_{o4} \left(Z_1 Z_{o1} + 2Z_2^2 + 2Z_1 Z_2\right)\right) \end{array} \right) \\ & -Z_{e1} Z_{e2} Z_{o2} Z_{o3} Z_{o4} Z_2 Z_{o1} \\ & \left(Z_{e2} Z_{e3} + Z_{e2} Z_{e4} + Z_{e3}^2\right) \end{aligned} \tag{A2}$$

$$\begin{aligned} A_2 = & Z_{o1} Z_{o2} (Z_1 Z_{o1} Z_{o3} Z_{o4} + Z_2 \left(2Z_1 + 2Z_2 + Z_{o1}\right) \\ & \left(Z_{o2} Z_{o3} + Z_{o2} Z_{o4} + Z_{o3}^2\right)) \\ & \left(Z_{e2} Z_{e3} Z_{e4} + Z_{e1} \left(Z_{e2} Z_{e3} + Z_{e2} Z_{e4} + Z_{e3} Z_{e4}\right)\right) \\ & +Z_{o1} Z_{o2} Z_2 Z_{o3} Z_{o4} \left(2Z_1 + 2Z_2 + Z_{o1}\right) \\ & \left(Z_{e3}^2 Z_{e4} + Z_{e3}^2 Z_{e5} + Z_{e3} Z_{e4}^2 + Z_{e1} Z_{e3}^2\right) \\ & + \left(\begin{array}{l} Z_1 Z_{o1} \left(Z_{o2} Z_{o3} + Z_{o2} Z_{o4} + Z_{o3} Z_{o4}\right) \\ +Z_{o1} Z_2 Z_{o3}^2 \left(2Z_1 + 2Z_2 + Z_{o1}\right) \\ +Z_{o2} \left(Z_{o2} Z_{o3} + Z_{o2} Z_{o4} + Z_{o3}^2\right) \\ \left(Z_1 Z_{o1} + 2Z_2^2 + 2Z_1 Z_2\right) \end{array} \right) \\ & Z_{e1} Z_{e2} Z_{e3} Z_{e4} \\ & v + \left(\begin{array}{l} Z_{o1} Z_2 \left(2Z_1 + 2Z_2 + Z_{o1}\right) \\ \left(Z_{o2} Z_{o3} + Z_{o2} Z_{o4} + Z_{o3} Z_{o4}\right) \\ +Z_{o2} \left(\begin{array}{l} Z_2 Z_{o1} \left(Z_{o2} Z_{o3} + Z_{o2} Z_{o4} + Z_{o3}^2\right) \\ +Z_{o3} Z_{o4} \left(Z_1 Z_{o1} + 2Z_2^2 + 2Z_1 Z_2\right) \end{array} \right) \end{array} \right) \\ & Z_{e1} Z_{e2} \left(Z_{e2} Z_{e3} + Z_{e2} Z_{e4} + Z_{e3}^2\right) \end{aligned} \tag{A3}$$

$$\begin{aligned} A_3 = & -Z_1 Z_{o1} Z_{o1} Z_{o2} \left(Z_{o2} Z_{o3} + Z_{o2} Z_{o4} + Z_{o3}^2\right) \\ & \left(Z_{e2} Z_{e3} Z_{e4} + Z_{e1} \left(Z_{e2} Z_{e3} + Z_{e2} Z_{e4} + Z_{e3} Z_{e4}\right)\right) \\ & -Z_{o1} Z_{o2} (Z_1 Z_{o1} Z_{o3} Z_{o4} + Z_2 \left(2Z_1 + 2Z_2 + Z_{o1}\right) \\ & \left(Z_{o2} Z_{o3} + Z_{o2} Z_{o4} + Z_{o3}^2\right)) \\ & \left(Z_{e3}^2 Z_{e4} + Z_{e3}^2 Z_{e5} + Z_{e3} Z_{e4}^2 + Z_{e1} Z_{e3}^2\right) \\ & +Z_1 Z_{o1} Z_{o1} Z_{o3}^2 Z_{e1} Z_{e2} \left(Z_{e2} Z_{e3} + Z_{e2} Z_{e4} + Z_{e3}^2\right) \\ & - \left(\begin{array}{l} Z_1 Z_{o1} \left(Z_{o2} Z_{o3} + Z_{o2} Z_{o4} + Z_{o3} Z_{o4}\right) \\ +Z_{o1} Z_2 Z_{o3}^2 \left(2Z_1 + 2Z_2 + Z_{o1}\right) \\ +Z_{o2} \left(Z_{o2} Z_{o3} + Z_{o2} Z_{o4} + Z_{o3}^2\right) \\ \left(Z_1 Z_{o1} + 2Z_2^2 + 2Z_1 Z_2\right) \end{array} \right) \\ & Z_{e1} Z_{e2} \left(Z_{e2} Z_{e3} + Z_{e2} Z_{e4} + Z_{e3}^2\right) \end{aligned} \tag{A4}$$

$$\begin{aligned} A_4 = & Z_1 Z_{o1} Z_{o1} Z_{o2} \left(Z_{o2} Z_{o3} + Z_{o2} Z_{o4} + Z_{o3}^2\right) \\ & \left(Z_{e3}^2 Z_{e4} + Z_{e3}^2 Z_{e5} + Z_{e3} Z_{e4}^2 + Z_{e1} Z_{e3}^2\right) \\ & +Z_1 Z_{o1} Z_{o1} Z_{o3}^2 Z_{e1} Z_{e2} (Z_{e2} Z_{e3} + Z_{e2} Z_{e4} + Z_{e3}^2) \end{aligned} \tag{A5}$$

REFERENCES

[1] Tang, C.-W. and C.-H. Yang, "New method for the microstrip bandstop filter with a wide stopband and an extremely high attenuation," *IEEE Transactions on Circuits and Systems II: Express Briefs*, Vol. 69, No. 11, 4318–4322, 2022.

[2] Rajput, A., M. Chauhan, and B. Mukherjee, "An ultra-wideband bandstop filter with circularly etched stub resonator," *Microwave and Optical Technology Letters*, Vol. 63, No. 12, 2958–2963, 2021.

[3] Liu, L., X. Liang, H. Fan, R. Jin, X. Bai, and J. Geng, "Compact wideband bandstop filter with directly controlled rejection," *IEEE Transactions on Circuits and Systems II: Express Briefs*, Vol. 68, No. 7, 2282–2286, 2021.

[4] Ramya, S. and I. S. Rao, "Design of compact ultra-wideband microstrip bandstop filter using split ring resonator," in *2015 International Conference on Communications and Signal Processing (ICCSP)*, 0105–0108, Melmaruvathur, India, 2015.

[5] Almansour, F. H., G. H. Alyami, M. A. Alshammari, and H. N. Shaman, "Ultra-wideband (UWB) microstrip bandstop filter with transmission zeros," in *2023 SBMO/IEEE MTT-S International Microwave and Optoelectronics Conference (IMOC)*, 106–108, Castelldefels, Spain, 2023.

[6] Rajput, A. and B. Mukherjee, "Compact microstrip bandstop filter for UWB application," *IETE Technical Review*, Vol. 41, No. 2, 123–132, 2024.

[7] Kong, M., Y. Wu, Z. Zhuang, Y. Liu, and A. A. Kishk, "Compact wideband reflective/absorptive bandstop filter with multi-transmission zeros," *IEEE Transactions on Microwave Theory and Techniques*, Vol. 67, No. 2, 482–493, 2018.

[8] Zuo, X. and L. Qin, "A novel approach to design wideband bandstop filter with wide upper bandpass bandwidth," *AEU — International Journal of Electronics and Communications*, Vol. 138, 153897, 2021.

[9] Chen, F. C., R. S. Li, J. M. Qiu, and Q. X. Chu, "Sharp-rejection wideband bandstop filter using stepped impedance resonators," *IEEE Transactions on Components, Packaging and Manufacturing Technology*, Vol. 7, No. 3, 444–449, 2017.

[10] Koirala, G. R., B. Shrestha, and N.-Y. Kim, "Compact dual-wideband bandstop filter using a stub-enclosed stepped-impedance resonator," *AEU — International Journal of Electronics and Communications*, Vol. 70, No. 2, 198–203, 2016.

[11] Xiao, J. K. and Y. F. Zhu, "Multi-band bandstop filter using inner T-shaped defected microstrip structure (DMS)," *AEU — International Journal of Electronics and Communications*, Vol. 68, No. 2, 90–96, 2014.

[12] Rajput, A., M. Chauhan, and B. Mukherjee, "A novel multi wideband bandstop filter with annular shaped stubs," *AEU — International Journal of Electronics and Communications*, Vol. 142, 153993, 2021.

[13] Rajput, A. and B. Mukherjee, "Electronically tunable UWB band stop filter using varactor diode," *AEU — International Journal of Electronics and Communications*, Vol. 164, 154610, 2023.

[14] Kanchana, D., S. Radha, B. S. Sreeja, and E. Manikandan, "A single layer UWB frequency selective surface for shielding application," *Journal of Electronic Materials*, Vol. 49, 4794–4800, 2020.

[15] Zhu, L., S. Sun, and R. Li, *Microwave Bandpass Filters for Wideband Communications*, John Wiley & Sons, 2011.